Friulian Journal of Science **38.** 2024, 29-48

Study of Climate Evolution Using Deterministic Object-based Numerical Models*

ENRICO MAIERO**, DARIO GIAIOTTI***

Abstract. Within the framework of climate change studies, an object-based climate model is developed and then used to study future climate scenarios. The Earth's surface is divided into five climate cells longitudinally: two polar cells, two temperate or Ferrel cells, and one equatorial or Hadley cell. This makes it possible to minimise the exchange of energy and matter between latitude bands: cells interact with each other only through energy exchanges, due to prevailing winds and dominant phenomena at the typical scale lengths of the interfaces between cells. These interfaces, which will be defined as secondary objects of the system, account for the nonlinear behaviour of the system.
The calibrated model, with plausible parameter values (except for an overestimated greenhouse-effect value), yields plausible and stable values for the temperatures of the five cells, although they fluctuate irregularly. It is likely that the inclusion of water vapour and the refinement of the system also correct the greenhouse gas parameter.
With the model, we simulate the growth of greenhouse gases, their historical growth and the growth projected by the IPCC (Intergovernmental Panel on Climate Change) RCPs (Representative Concentration Pathways)(see IPCCa n.d. and IPCCb 2018), albeit only qualitatively. The model shows its limitations particularly in the most optimistic cases

* This article is an excerpt from Enrico Maiero's Master's degree thesis, entitled *Studio dell'evoluzione climatica tramite modelli numerici deterministici ad oggetti* (Study of climate evolution using deterministic object-based numerical models), developed under the supervision of Prof. Dario Giaiotti while E.M. was an undergraduate student at the Department of Physics, University of Trieste.

** Department of Environmental Science, Computer Science and Statistics, *Ca' Foscari University* of Venice and National Institute of Oceanography and Applied Geophysics (OGS), Italy. Email: emaiero@ogs.it.
** Department of Physics, University of Trieste, Italy. Email: dgiaiotti@units.it.

proposed by the IPCC, that is, if the forcing, after being increased, drops to its initial values again: the retarding effect of the oceans cannot be considered. It is, however, credible to simulate negative impulsive forcings.
Of particular interest is the overlapping of the temperatures of the three central cells in cases of high system forcings: this may be due to the Hadley cell's attempt to expand, which it is prevented from doing by the fixed geometry of this version of the model.
Due to its computational efficiency, the model lends itself to ensemble simulations. In addition, the secondary objects considered correspond to extreme weather events, so the model is suitable for assessing whether, as a result of climate change, these will increase in number and intensity.

Keywords. Object-based climate models, atmospheric circulation cells, climate change.

1. Introduction.

The international scientific community agrees that climatic changes are taking place, which have a strong correlation with global warming caused by the emission of greenhouse gases (primarily carbon dioxide and methane) produced by human activities. Understanding the evolution of the atmosphere – which is part of the climate system – under the pressure of human activities, has thus become a matter of great importance. To do this, reduced-complexity models that emphasise cause-and-effect relations can be used with good results. In this context, the object-oriented model was developed and subsequently used for simulations of climate change by introducing an arbitrary forcing, including according to scenarios outlined by the IPCC (2018).

2. Materials and methods

2.1. The model. Earth's atmosphere is divided into five main objects in the longitudinal direction, which correspond to climate cells: two polar cells, two temperate or Ferrel cells, and one equatorial or Hadley cell. The latter is actually made up of two cells, one in each hemisphere. However, for the purposes of this study, it is more practical to consider them as one cell. Cells are characterised by a closed circulation: it can therefore be assumed, as a first approximation, that there is an exchange

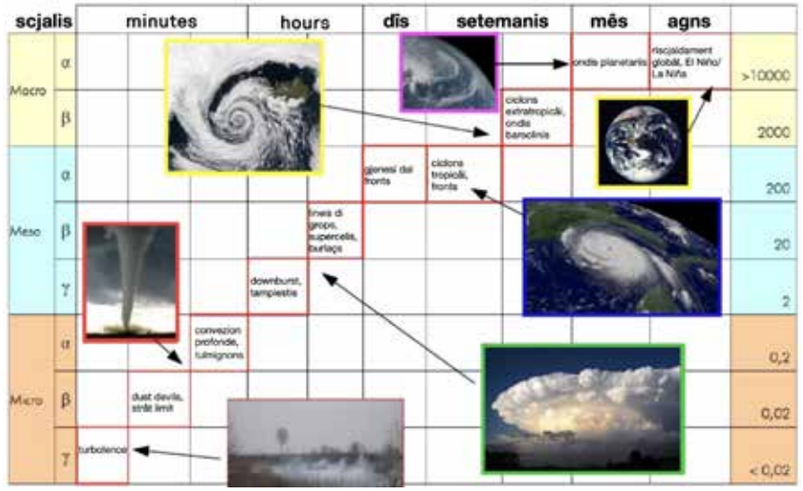

Figure 1. Comparison of the scales of tropical cyclones and extratropical cyclones, which are associated with Rossby waves. The former are placed in the mesoscale, the latter in the macroscale. In all cases, these are *synoptic scale* phenomena. Source: Giaiotti (2017, 2018, 2019).

of energy, but not an exchange of mass, between them. This exchange of energy takes place through the action of prevailing winds (mid-latitude westerlies and trade winds) and dominant atmospheric phenomena on the typical scales of cell interfaces (thousands or tens of thousands of kilometres): tropical cyclones at low latitudes and Rossby waves at high latitudes were identified (Fig. 1). In the model presented here, these phenomena are called secondary objects of the system.

This produces a dynamic system consisting of five differential equations that have as dynamic variables the average temperatures of the five cells at a given time τ, that is, in the integration step:

$$c^i \frac{\mathrm{d}T^i}{\mathrm{d}t} = \mathbf{A}^i - \mathbf{B}^i + \mathbf{C}^i + \mathbf{D}^i \tag{2.1}$$

The dynamic system thus lives in a phase space of five dimensions.

The terms in the equations have the dimensions of energy flux: the unit of measurement is therefore $\mathrm{W} \cdot \mathrm{m}^{-2}$ and the values used are average values over the areas of the cells (Table 2) and on the time step τ, which we leave undetermined for the moment. The index $i \in \{0, 1, 2, 3, 4\}$

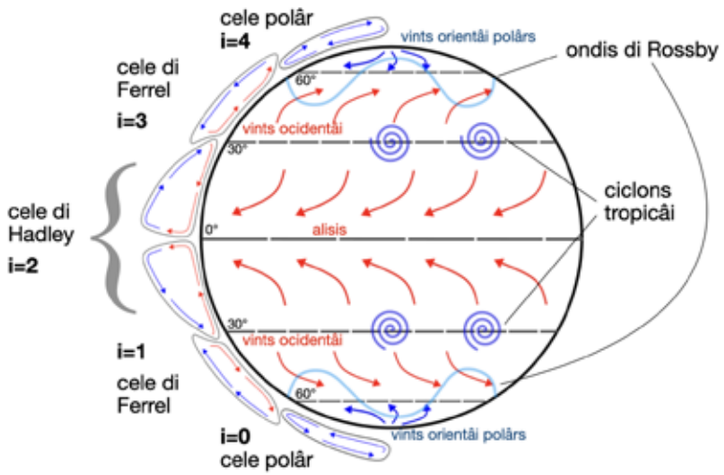

Figure 2. Diagram showing the division of the Earth into the cells used in the object-based climate model. The five cells dividing the planetary surface longitudinally are the *main objects* of the model. There are two Hadley cells but, for computational simplicity, only one is considered in the model. The prevailing winds are also shown: trade winds in Hadley cells, westerly winds in Ferrel cells, and polar easterly winds. The indices actually used in the model are shown. The colours from blue to red represent cell temperatures, from lowest to highest. The boundaries between the Hadley and Ferrel cells are set at 30° latitude (north and south), where tropical high pressures are found. In contrast, the boundary between each Ferrel cell and its polar cell is set at the latitude of the polar circle (66°33′39″). (Lutgens, Tarbuck e Tasa, 2007)

(which is clearly not an exponent) is referred to the cell: for $i = 0$ we have the southern polar cell, and so on up to $i = 4$ (Fig. 2). On the left in the equation appears the first derivative of temperature over time. The temperature is the average temperature of each cell, over the area and time step. The constant c^i is the surface heat capacity of each cell. On the right, instead, there are four terms, namely the contributions to the energy balance:

- Incoming radiation:

$$\mathbf{A}^i = g^i S(1 - \alpha^i) \tag{2.2}$$

  with S the solar constant, g^i the geometric factor of the cell (integral over the cell of the scalar product between the direction of radiation incidence and the vector orthogonal to the surface, all divided by the area of the cell), and α^i the albedo of the cell;

- Outgoing radiation:

$$\mathbf{B}^i = m\sigma T^4(1 - \beta) \tag{2.3}$$

  with σ the Stefan-Boltzmann constant, m the relative emissivity, β the fraction of radiation retained by the greenhouse effect;

- Heat transport between cells:

$$\mathbf{C}^i = (C^i_{North} l^i_{North} + C^i_{South} l^i_{South}) \frac{h^i}{A^i} \tag{2.4}$$

  where h^i is the mean height of the troposphere in the cell, A^i is the surface area of the cell, $C^i_{North,South}$ is the sensible heat coming from the adjacent, northern or southern, cell and is composed of two contributions:

$$C^i_{North,South} = C^{i,CONT}_{North,South} + C^{i,OGG}_{North,South} \tag{2.5}$$

  where

  – the first term is continuous and is due to the prevailing winds (trade winds, westerly winds of mid-latitudes):

$$C^{i,CONT}_{North,South} = -\text{sgn}(T^i - T^{i\pm1}) K^i_{North,South} f^i(|T^i - T^{i\pm1}|) \tag{2.6}$$

    and

  – the second to secondary objects and is the product of their number and intensity:

$$|C^{OGG}| = n_{ogg}(|\Delta T|) int_{ogg}(|\Delta T|) \tag{2.7}$$

    * Tropical cyclones, between the Hadley and Ferrel cells, are activated only if $T^{Hadley} = T^{i=2} > T^{Ferrel}$ and $T^{Hadley} = T^{i=2} > T_{cycl}$, where T_{cycl} is a critical temperature for tropical cyclone activation[1], and the term expressing their contribution should be subtracted from the central cell

[1] This is meant to represent the fact that tropical cyclones are triggered by sea surface temperatures above 26 °C (Tory and Dare, 2015), but the sea is not represented here, so a value for atmospheric temperature is used.

and added to the temperate ones:

- Number:

$$n_{cycl} = \text{floor}(\eta_{cycl}((T^{Hadley} - T_{cycl})\epsilon_{cycl} + 1)^{\lambda_{nC}}) \tag{2.8}$$

The number has an upper limit in the ratio between the length of the parallel to the boundary between the central cells and the typical diameter of a cyclone, for a corrective parameter.

- Intensity:

$$int_{cycl} = int^{min}_{cycl}((T^{Hadley} - T_{cycl})\epsilon_{cycl} + 1)^{\lambda_{iC}} \tag{2.9}$$

* Rossby waves, between Ferrel and polar cells, are activated only if $T^{polar} < T^{Ferrel}$:

- Number:

$$n_R = \text{int}(\eta_{nR}(|T^{Ferrel} - T^{polar}|)^{\lambda_{nR}}) \tag{2.10}$$

- Intensity:

$$int_R = \eta_{iR}(|T^{Ferrel} - T^{polar}|)^{\lambda_{iR}} \tag{2.11}$$

- Latent heat:

$$\mathbf{D}^i = L_v \Delta e^i \tag{2.12}$$

with L_v the latent heat of condensation/evaporation and Δe^i the net condensed vapour fraction (in case of evaporation, this quantity has a negative sign). In any case, considering that solving this term would also require matching equations for water vapour transport, it was preferred, for this preliminary study, to set it to 0.

The model thus described is summarised in Table 1. The most complex term is definitely that of heat transport, which consists of a continuous contribution (the prevailing winds, such as the Trade Winds) and a noncontinuous contribution (the secondary objects), which are activated only if a certain temperature threshold is exceeded and, in the case of tropical cyclones, only if the temperature of the Hadley cell is higher

Table 1. Summary of the energy balance equation for a cell in the object-based model. The index i denotes the cell, i growing northward. The physical meaning of the parameters is illustrated in Table 2. It should be noted that: 1) if $i = 0$, the terms with index $i-1$ are set equal to 0; if $i = 4$, the terms with index $i+1$ are set equal to 0; 2) the temperature differences that form the basis of the exponentials should be considered dimensionless because they are normalised by an appropriate factor, which is worth 1 in the modulus, unless otherwise specified.

Energy balance of the i-th cell $c^i \frac{dT^i}{dt} = \mathbf{A}^i - \mathbf{B}^i + \mathbf{C}^i + \mathbf{D}^i$	
Incoming shortwave radiation	$\mathbf{A}^i = g_i S(1 - \alpha_i)$
Outgoing longwave radiation	$\mathbf{B}^i = m\sigma T^4(1 - \beta)$
Sensible heat transport	$\mathbf{C}^i = \sum_{\substack{j=nord,\\ sud}} C^i_j l^i_j \frac{h^i}{A^i}$
Surface density of sensible heat	$C^i_{nord,sud} = C^{i,CONT}_{nord,sud} + C^{i,OGG}_{nord,sud}$
Contrib. of prevailing winds	$C^{i,CONT}_{nord} = -\text{sgn}(T^i - T^{i+1})K^i_{nord}(\lvert T^i - T^{i\pm1}\rvert)^{\gamma^i_{nord}}$ $C^{i,CONT}_{sud} = -\text{sgn}(T^i - T^{i-1})K^i_{sud}(\lvert T^i - T^{i\pm1}\rvert)^{\gamma^i_{sud}}$
Contrib. of secondary objects:	$\lvert C^{OGG}\rvert = n_{ogg}(\lvert\Delta T\rvert) int_{ogg}(\lvert\Delta T\rvert)$
-tropical cyclones	They appear only if $T^{Hadley} = T^{i=2} > T^{Ferrel}$ & $T^{Hadley} = T^{i=2} > T_{cycl}$
	Subtract for $i = 2$, add for $i = 1$ o $i = 3$
	$n_{cycl} = \text{floor}(\eta_{cycl}((T^{Hadley} - T_{cycl})\epsilon_{cycl} + 1)^{\lambda_{nC}})$, but if $n_{cycl} > \frac{l^{Hadley}}{L^{min}_{cycl}}\xi$ then $n_{cycl} := \frac{l^{Hadley}}{L^{min}_{cycl}}\xi$
	$int_{cycl} = int^{min}_{cycl}((T^{Hadley} - T_{cycl})\epsilon_{cycl} + 1)^{\lambda_{iC}})$
-Rossby waves	They appear only if $T^{polar} < T^{Ferrel}$
	Subtract for $i = 1$ o $i = 3$, add for $i = 0$ o $i = 4$
	$n_R = \text{int}(\eta_{nR}(\lvert T^{Ferrel} - T^{polar}\rvert)^{\lambda_{nR}})$
	$int_R = \eta_{iR}(\lvert T^{Ferrel} - T^{polar}\rvert)^{\lambda_{iR}}$
Contribution due to condensation/evaporation	$\mathbf{D}^i = L_v \Delta e^i$

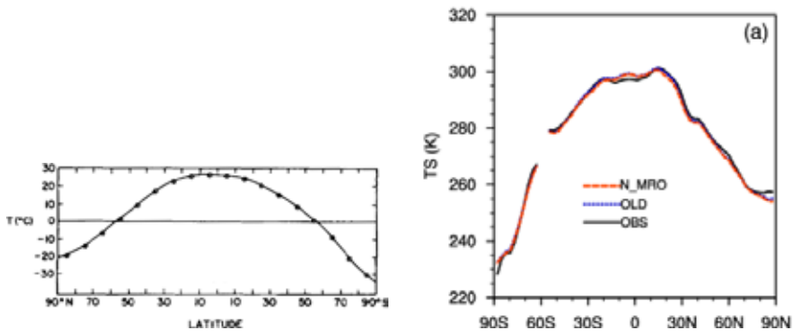

Figure 3. Temperature as a function of latitude as predicted by various models in the existing literature. (a) Graphic reworking taken from Sellers (1969), temperature in Degrees Celsius; (b) (Zhang, Jing e Li, 2014), temperature in Kelvin.

than that of the neighbouring cell. In addition, secondary objects appear in discrete numbers even though their energy may vary continuously.

2.2. Model calibration. Within the equations, parameters appear, whose meanings are listed in Table 2. Plausible values of the parameters were obtained through a model calibration procedure. For this task, two criteria were followed. Firstly, a search was conducted in the scientific literature for already existing estimates of the parameter values or related quantities. Subsequently, a refinement was carried out, adjusting parameter values within plausible ranges and running the program that implements the model, until convergence to realistic values for the temperatures of the five cells was achieved. This value was estimated from the graphs in Figure 3: 292K for the Hadley cell, 287K for the Ferrel cell (preferring the northern Ferrel cell to be just a little colder), 272K for the northern polar cell, 265K for the southern polar cell, with tolerance

Table 2. Parameters that appear in the energy balance equation for a cell of the object-based model: showing their names, symbols, and calibration values as described in section 2.2. The first part of the table covers geometric quantities and physical constants that are valid apart from calibration; the second part covers calibrated quantities. Superscript i is placed on the dependent quantities of the cell.

Size	Symbol	Value
Stefan-Boltzmann constant	σ	$5.67 \cdot 10^{-8}\mathrm{W} \cdot \mathrm{m}^{-2}\mathrm{K}^{-4}$
Average radius of the Earth	R_T	$6.37 \cdot 10^{6}\mathrm{m}$
Latitude of the Hadley-Ferrel boundary	ϕ^{Hadley}	$30°$
Latitude of the Ferrel-polar cell boundary	ϕ^{polar}	$66°33'39''$
Height of the atmosphere in the cell	h^i	$[8.0; 12; 18; 12; 8.0] \cdot 10^{3}\mathrm{m}$
Latent heat of evaporation of water	L_v	$2.27 \cdot 10^{6}\mathrm{J} \cdot \mathrm{kg}^{-1}$
Solar constant	S	$1370\mathrm{W} \cdot \mathrm{m}^{-2}$
Earth Emissivity	m	0.964
Albedo	α^i	$[0.26; 0.30; 0.35; 0.35; 0.25]$
Surface heat capacity	c^i	$[17; 20; 20; 19; 18]\mathrm{J} \cdot \mathrm{m}^{-2}$
Coeff. for sensible heat (prev. winds)*	K^i_{nord}	$[15; 40; 40; 15; 0]\mathrm{J} \cdot \mathrm{K}^{-1}$
Expon. for sensible heat (prev. winds)*	γ^i_{nord}	$[0.4; 1.2; 1.2; 0.5; 0]$
Fraction of longwave rad. retained**	β	0.46
Temp. threshold for tropical cyclones	T_{cycl}	296K
Coeff. for ΔT in the no. of tropical cyclones	η_{cycl}	40
Normalization factor for ΔT for trop. cycl.	ϵ_{cycl}	$1\mathrm{K}^{-1}$
Expon. for the no. of tropical cyclones	λ_{nC}	1.5
Minimum length of a tropical cyclone	L^{min}_{cycl}	$2.0 \cdot 10^{6}\mathrm{m}$
Correction factor for no. of trop. cyclones	ξ	3
Minimum intensity of a tropical cyclone	int^{min}_{cycl}	$10\mathrm{W} \cdot \mathrm{m}^{-2}$
Exponent for tropic. cyclone intensity	λ_{iC}	4
Coeff. for ΔT in the no. of Rossby waves	η_{nR}	31.5
Exponent for the no. of Rossby waves	λ_{nR}	0.5
Coeff. for ΔT in the intensity of R. waves	η_{iR}	15
Exp. for int. of N. hemisphere R. waves	λ_{iR}	1.7
Exp. for int. of S. hemisphere R. waves	λ_{iR}	1.5

*We refer the array for exchanges with cells to the north; to get K^i_{sud} one simply translates the array values cyclically to the right. The parameters have no sign: the sign is determined by the temperature.
**Manual calibration of β leads to overestimation of the quantity: the correct figure should be calculated by taking a simple energy balance model for the entire planet as reference.

set at approximately 2K.

The first part of Table 2 consists entirely of well-known physical constants, which did not need to be calibrated; the second part, however, comprises the calibrated quantities. We see that one can easily derive the area of a cell between two latitudes φ_0 e φ_1:

$$2\pi R_T^2(\sin(\varphi_1) - \sin(\varphi_0)) \tag{2.13}$$

In the same way, also the g^i factor in equation 2.2:

$$g^i = \frac{\varphi_1 - \varphi_0 + \sin(\varphi_1)\cos(\varphi_1) - \sin(\varphi_0)\cos(\varphi_0)}{2\pi(\sin(\varphi_1) - \sin(\varphi_0))} \tag{2.14}$$

Given that the value chosen for the solar constant S is an annual average, the time step can be taken on the order of one year: $\tau \gtrapprox 1yr$ [2].

An example of the way the parameters were calibrated is that of tropical cyclones: since $\tau \gtrapprox 1yr$ and there are a few dozen tropical cyclones in a year (see e.g. WMOb), one would expect η_{cycl} to be a few dozen. Furthermore, knowing that the (*Convective Available Potential Energy* (CAPE) in the boundary layer of an area subjected to a cyclone is $2000\mathrm{J}\cdot\mathrm{kg}^{-1}$ (Lee e Frisius 2018) and considering the magnitude-scale typical of a tropical cyclone, it is possible to estimate the power to be about 10^{14}W and thus values of tropical cyclone parameters that produce powers between 10^{12}W and 10^{15}W.

The parameter η_{nR}, the number of Rossby waves, can be 7. Considerations of energies and temperatures included provide the values in Table 2.

The albedo and heat capacity values found in the literature (Schwartz 2007) are, for the entire planet, $\alpha = 0.31$, $C = 17\mathrm{J}\cdot\mathrm{m}^{-2}$. The values of the individual cells were derived by taking, as references, the planetary values as average values and considering the differences and asymmetries between cells. For example, the presence of ice and continental clouds raises the albedo, but weak solar rays result in a weak albedo (and this explains the low values for polar cells); in other words, large amounts of water increase heat capacity. Similar considerations have also been made for other quantities, taking into account the asymmetries between

[2]This is a sensible choice when studying the climate, since climate can be defined as the average behaviour of the atmosphere over a very long time interval, usually thirty years (see WMOa)

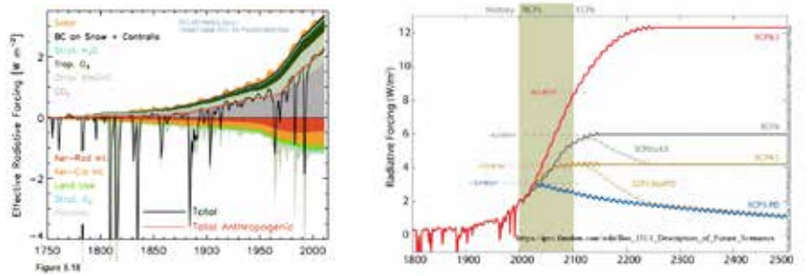

(a) **(b)**

Figure 4. (a) Growth of radiative forcing over the past two and a half centuries. One can see the importance of carbon dioxide's contribution. The surge of the curve from 1960 onwards inspired the name of the curve: *hockey stick*. Source: IPCC (2018). (b) Growth of radiative forcing over the past two and a half centuries, extrapolated to show future climate scenarios under different policy choices regarding carbon dioxide emission control. The years of this century, which are critical for the future, are highlighted. Source: IPCC (2018)

.

the two hemispheres.

The values obtained are shown in the last column of Table 2. The only parameter that is calibrated to a value far from those measured is β, which represents the fraction of longwave radiation retained by the system due to the greenhouse effect: the value estimated on the basis of observation is $\beta_{oss} = 0.36$, the one obtained by calibration $\beta_{cal} = 0.46$.

2.3. Case Study. A forcing term ΔF can be introduced into the equations, so in this case the equations become:

$$c^i \frac{\mathrm{d}T^i}{\mathrm{d}t} = \mathbf{A}^i - \mathbf{B}^i + \mathbf{C}^i + \Delta F + \mathbf{D}^i \tag{2.15}$$

with the same meaning as the symbols in Section 1.

The forcing term is useful in that it permits the inclusion, in each cell's energy balance, of elements that are external to the system but which may affect the system itself, such as a volcanic eruption or emissions resulting from anthropic activities. For the study being presented, forcings of different types were included: a constant term over time, one that increased linearly for a given time and then remained constant, and one that increased in a hockey-stick fashion i.e. according to the hockey-

stick shaped graph showing the greenhouse gases (carbon dioxide and methane) trend over time (Fig. 4a) (two linear increases, first a slower one, then a faster one, and then a constant value).

Also included are two forcings that have similar trends qualitatively to the future scenarios developed by the IPCC, specifically the well-known *Representative Concentration Pathway* (RCP) (ICCPb 2018). From a qualitative point of view, the hockey stick growth projected into the future is isomorphic to the worst-case scenarios, while, in contrast, the best-case scenarios follow a linear decrease. This latter case was also simulated (Fig. 4b).

Finally, we see what is involved in impulsive negative forcing, such as those produced by volcanoes erupting so strongly that they send particulate matter into the stratosphere. The negative pulse is followed by a linear growth to the original value of the forcing, representing the fall of particulate matter.

By doing these numerical experiments, we see the response of cell temperatures, intensity, and number of secondary objects for each time step following an alteration in the forcing.

The model was implemented in Python language (Python Software Foundation).

3. Results. Figure 5 shows the time series (the time unit set as the step size τ) of cell temperatures for different simulations.

The behaviour of the calibrated model can be seen in Figures 5a, where the secondary objects were not activated, and 5b, where they were activated. In both cases, a 200-year model run was performed. In the first case, the temperatures assume constant values after a transient, so that the trajectories in phase space fall back to an equilibrium point; in the second case, the temperatures of the five cells fluctuate around average and plausible values, although these fluctuations are not regular, so the trajectories in phase space fall on a strange attractor. It is evident that it is the secondary objects that introduce the non-linearity of the system. In addition, secondary objects increase the efficiency of energy transport, consequently the cell temperatures are closer together in Figure 5b than in 5a.

Image 6a shows the numbers of cyclones and Rossby waves that are obtained for the calibrated model. Note that cyclones always oscillate

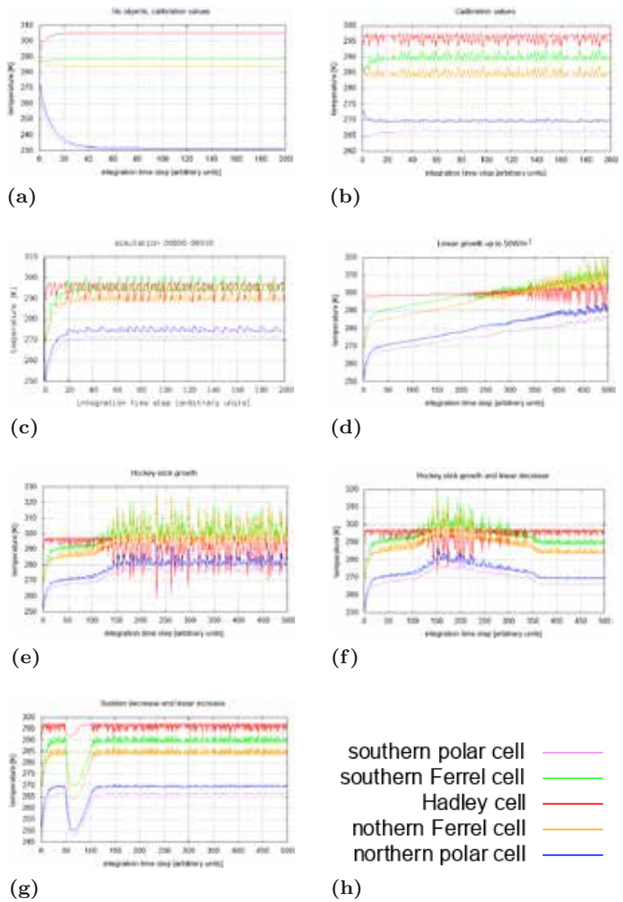

Figure 5. Results of simulations. Evolution of cell temperature over time, for model calibration values shown in Table 2 unless otherwise specified. (a) The contributions of secondary objects (cyclones and Rossby waves) are set to zero. (b) Secondary objects are "activated" (parameters at calibration values). (c) Constant forcing $10\mathrm{W m}^{-2}$. (d) $\lambda_{iC} = 2$ and the forcing varies linearly with time from 0 to $50\mathrm{W} \cdot \mathrm{m}^{-2}$ in 500 integration steps. (e) The forcing varies linearly with time according to a step function: in the first 100 iterations from $0\mathrm{W} \cdot \mathrm{m}^{-2}$ to $5\mathrm{W} \cdot \mathrm{m}^{-2}$, in the next 50 from $5\mathrm{W} \cdot \mathrm{m}^{-2}$ to $20\mathrm{W} \cdot \mathrm{m}^{-2}$, and finally stops at this value. (f) The forcing varies linearly with time according to a step function: in the first 100 iterations from $0\mathrm{W} \cdot \mathrm{m}^{-2}$ to $5\mathrm{W} \cdot \mathrm{m}^{-2}$, in the next 50 from $5\mathrm{W} \cdot \mathrm{m}^{-2}$ to $20\mathrm{W} \cdot \mathrm{m}^{-2}$, in the next 200 it drops again to $0\mathrm{W} \cdot \mathrm{m}^{-2}$, and finally stops at this value. (g) The forcing drops in impulsive mode to $-50\mathrm{W} \cdot \mathrm{m}^{-2}$ to $5\mathrm{W} \cdot \mathrm{m}^{-2}$ at the 50-th iteration and rises linearly to $0\mathrm{W} \cdot \mathrm{m}^{-2}$ in 50 iterations, to finally stop at this value. (h) Legend.

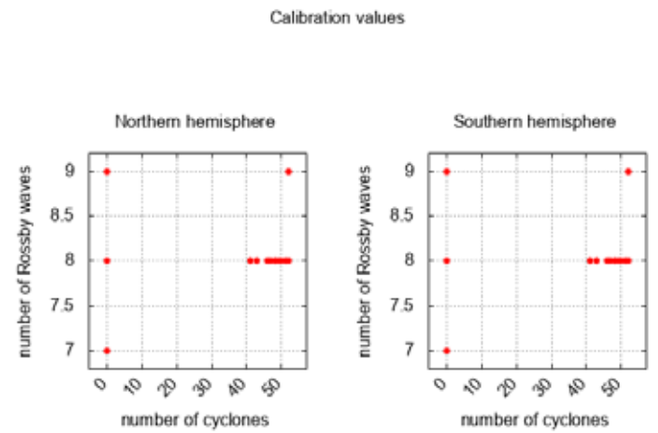

(a)

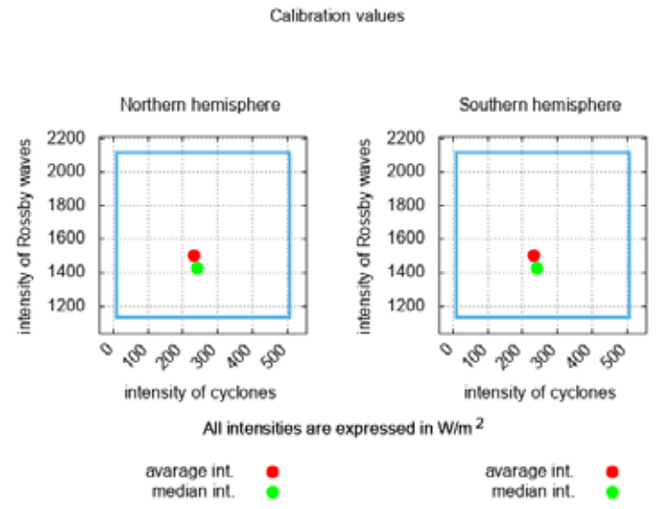

(b)

Figure 6. Numerical results for one *run* of the calibrated climate model (Table 2, , initial temperature as in Figure 5b) tin the two hemispheres. (a) Number of tropical cyclones vs. number of Rossby waves. (b) Intensity of tropical cyclones vs. intensity of Rossby waves. The red dot (the point placed higher in the Figure) lies on the mean values of both magnitudes, the green dot (the point placed lower in the Figure) is the median; the light blue rectangle is plotted between the minima and maxima of the intensity.

between 0 and values close to the maximum, where – in contrast – Rossby waves are in practice always present in nearly constant amounts. Figure 6b shows the energies of cyclones and Rossby waves.

If a constant forcing term ΔF is introduced, the temperatures of noncentral cells all rise, but the effect is much more pronounced in polar cells. The Hadley cell, on the other hand, cannot raise its temperature since, whenever the T_{cycl}, temperature is exceeded, the cell is forced to give up excess energy by way of cyclones. At high forcing values, the temperatures of the Hadley and Ferrel cells tend even to coincide. All this can be seen in Figure 5c. intensity of secondary objects increases as the forcings increase, while the number always fluctuates between 0 and a maximum value.

With a forcing that grows linearly over time (a situation that may simulate a constant increase in GHGs) we find the same characteristics already seen in constant forcings, both with respect to temperature and secondary objects; it is clear that the oscillations become gradually larger and less realistic as time progresses (Fig. 5d).

The realistic trend of the radiative forcing is, as already mentioned, that of the *hockey stick* (Fig. 4a); simulating such growth according to a forcing that remains constant at the final value (as also corresponds to the future scenarios without reabsorption of the forcing in Fig. 4b), , we once again have the two-slope trend in cell temperatures (Fig.5e). The other type of future scenarios in Figure 4b is that which, after hockey stick growth, has the forcing decreasing linearly over time to preindustrial values. Here too, the cell temperatures reflect the forcing trend (Fig. 5f).

Finally, by applying a negative impulsive forcing and after a short linear growth up to the initial situation, we see that the temperatures suddenly drop, but over long time periods there is no memory of this effect (Fig. 5g).

4. Discussion. A first note should be made about the calibration of the model: there is certainly ample room for improvement, perhaps by searching for more up-to-date data and looking at the statistical distributions of the results that are obtained by means of the model (analysing, for example, the time series obtained and comparing these with those observed). In addition, some parameters are actually temperature-depen

dent, like albedo, which is highly dependent on the cloudy surface area and the frozen one. If all this is taken into account, it is likely that the β (see Table 2) can be calibrated more realistically.

With regard to the exhibited results, it should be mentioned that in the case of future scenarios and, more generally, in all cases where the forcing term ΔF, was used, it was preferable to look at the qualitative development of the system rather than trying to obtain precise numerical results, so the results should not be understood as predictions or indications of future climate.

A first consideration regarding the model, is that the function of secondary objects in introducing nonlinear behaviour of the system is fundamental. In fact Figures 5a and 5b show clearly how without secondary objects the attractor is a point of equilibrium, while with secondary objects it is a strange attractor and the temperatures always oscillate erratically. If we then also look at the number of Rossby waves and tropical cyclones (Fig. 6a), , we can clearly see that the former are always present while the latter are either absent or present in substantial numbers. This raises the suspicion that, although in theory neither of the two secondary objects is linear, it is the latter that are really responsible for the chaotic behaviour. In fact, confirmation of this was obtained by turning off Rossby waves and tropical cyclones separately. This behaviour is much clearer if we consider that cyclones, in order to ignite, require a given temperature threshold T_{cycl}.

Still referring to the number of tropical cyclones (Fig. 6a), you can also see that they are present either in numbers close to the maximum, or not present at all. This is unrealistic and is definitely a weakness of the model. The energies of secondary objects (Fig. 6b), on the other hand, are realistic, at least as an initial approximation.

Another limitation of the model is seen by introducing high forcings, such as the one in Figure 5c: Hadley and Ferrel cell temperatures tend to coincide, because the Hadley cell is forced to give up excess energy whenever it exceeds the T_{cycl} temperature. This almost certainly unrealistic result, however, can be interpreted in an interesting way: it could be explained as an attempt by the Hadley cell to enlarge, which it is not allowed to do because the geometry of the model is stable. If the Hadley cell could engulf neighbouring ones, which would mean admitting that the system has a variable geometry, one could think that the

global warming effect involved the widening of the Hadley cell and the shrinking of others, with a much clearer temperature-increasing effect in the polar cells.

With reference to the situation in Figure 5f, that is a scenario in which the forcing decreases after an increase, it is not credible that cell temperatures would immediately return to baseline levels, as the model suggests. This is because non-atmospheric components of the climate, such as the oceans, which have much longer reaction times, are not considered. The response to negative impulses, on the other hand, is realistic (see Figure 5g).

Finally, a necessary step for improving the model would be the inclusion of water vapor transport and phase transitions.

Clearly, you can expand the model with other secondary objects as well, such as monsoons. It is a strength of the model that secondary objects are linked to extreme weather events, which is why a study on the evolution of the number and strength of secondary objects may prove useful in investigating the effects of climate change on hydrometeorological risk.

The computational efficiency of the model makes it suitable for use in sets of simulations or in very long simulations.

In this paper, we wanted to give relevance to the physical results of the study and especially to the temperatures of the five cells in the different scenarios. In our thesis, we also looked at the properties of the secondary objects in different situations as well as a study of the model from the perspective of the dynamic system, studying the different topologies of the phase space with varying parameters and paying special attention to bifurcations[3]. Please refer to the thesis for any further details.

5. Conclusions. Secondary objects, particularly tropical cyclones, are responsible for the nonlinear behaviour of cell temperatures and play a key role in energy transport.

An object-based climate model was devised, calibrated and studied, in which the Earth is represented by means of five main objects, the climate cells (the equatorial or Hadley cell, the temperate or Ferrel cells,

[3]Those critical parameter values that make possible the switch from one topology to another, known as *bifurcation*

and the polar cells), which communicate with each other through energy transport by way of prevailing winds and secondary objects, namely tropical cyclones and Rossby waves. The model is a middle ground between dimension 0 models, which treat the planet as a thermodynamic system exchanging energy with outer space, with no internal dynamics of its own, and dimension 1 models, where we have the dimension of latitude. The advantage of the object-based model over 0-dimension models is that it represents atmospheric dynamics, even with a parameterization; compared to 1-dimension models, it simplifies the dynamics as much as possible, taking advantage of the fact that climate cells are more closed systems than arbitrary latitude bands.

A good result of the model is that, for realistic values of the initial temperatures and parameters (Table 2), , the system converges on a fixed point or a strange attractor in which the orbits move around realistic temperature values.

A second positive result is the plausible intensity of secondary objects, even with respect to transport due to prevailing winds; their behaviour is not as good, however, as it always fluctuates between 0 and a maximum value.

The calibration of the model highlights how the use of objects that contribute to the redistribution of energy in the global atmosphere, increases the efficiency of transport and introduces perturbations in the evolution of the dynamic system. In particular, the topology of the model solutions in phase space changes from a fixed point to a strange attractor, showing temperatures for each cell very close to those of the current Earth's atmosphere.

A third positive result, is that with plausible parameter values, the system converges to the right equilibrium temperatures. The only parameter that is calibrated to a value far from those measured is β, which represents the fraction of longwave radiation retained by the system due to the greenhouse effect. The value estimated on the basis of observation is $\beta_{oss} = 0.36$, while that obtained by calibration is $\beta_{cal} = 0.46$.

A fourth positive result is the behaviour of the system in response to the insertion of a climate forcing. A climate forcing similar to that of the greenhouse effect implies that the temperature rises in all cells, but mostly those at high latitudes (this agrees with scenarios developed by the community of climatologists [IPCCb 2018]); an impulsive climate

forcing, such as that of a volcanic eruption, has no lasting effects. Simulating global warming reveals the weak point of the model, namely the behaviour of the Hadley cell, which releases a lot of energy to the other cells whose meridional thermal gradient is reversed several times. In any case, this can be explained by the Hadley cell's attempt to enlarge to the detriment of neighbouring cells.

In conclusion, the model seems promising, so much so that, having corrected its main limitations (transport and phase change state of water vapour, switching to variable geometry, refining the parameters and making them temperature-dependent), one could consider using it to simulate ongoing climate changes, given also the advantage of its computational efficiency that favours the use of sets of simulations. One could pay close attention to how the number and intensity of secondary objects vary, considering that they are related to extreme weather events.

Acknowledgements

The authors sincerely thank Silvia Cipriani, Engineer, for her valuable assistance with the graphics.

References

Giaiotti D. (2018). *Lezions di Fisiche de Atmosfere*. Dipartiment di Fisiche. Universitât di Triest. Agns academics 2017–2018 e 2018–2019.

Intergovernmental Panel on Climate Change (IPCCa). https://www.ipcc.ch

(IPCCb 2018). Myhre G., Shindell D. Chapter 8: Anthropogenic and natural radiative forcing supplementary material. In IPCC AR5 Report. IPCC.

Lee M., Frisius T. (2018). On the role of convective available potential energy (CAPE) in tropical cyclone intensification. *Tellus A: Dynamic Meteorology and Oceanography*, 70(1).

Lutgens F. K., Tarbuck E. J., Tasa D. G. (2007). *The Atmosphere: An Introduction to Meteorology*. 10th edition.

Python Software Foundation. (c.d.). *Python*. Retrieved from https://www.python.org

Schwartz S. E. (2007). Heat capacity, time constant, and sensitivity of Earth's climate system. *Journal of Geophysical Research: Atmospheres*, 112(D24).

Sellers W. D. (1969). A global climatic model based on the energy balance of the Earth–atmosphere system. *Journal of Applied Meteorology*, 8(3), 392–400.

Tory K. J., Dare R. A. (2015). Sea surface temperature thresholds for tropical cyclone formation. *Journal of Climate*, 28(20), 8171–8183.

World Meteorological Organization (WMO). (c.d.). *Climate*. Retrieved from https://public.wmo.int/en/our-mandate/climate

World Meteorological Organization (WMO). (c.d.). Tropical Cyclones. Retrieved from https://public.wmo.int/en/our-mandate/focus-areas/naturalhazards-and-disaster-risk-reduction/tropical-cyclones

Zhang H., Jing X., Li J. (2014). Application and evaluation of MCICA scheme with new radiation code in BCC AGCM2.0.1. *Geoscientific Model Development*, 7(3), 737–754.